ACS APPLIED MATERIALS & INTERFACES

www.acsami.org

Research Article

Toward Sustainable Tackling of Biofouling Implications and Improved Performance of TFC FO Membranes Modified by Ag-MOF Nanorods

S. Fatemeh Seyedpour,[▽] Mostafa Dadashi Firouzjaei,[▽] Ahmad Rahimpour,[*] Ehsan Zolghadr, Ahmad Arabi Shamsabadi, Parnab Das, Farhad Akbari Afkhami, Mohtada Sadrzadeh, Alberto Tiraferri, and Mark Elliott[*]

Cite This: *ACS Appl. Mater. Interfaces* 2020, 12, 38285−38298

Read Online

ACCESS | Metrics & More | Article Recommendations | Supporting Information

ABSTRACT: In this work, nanorods with high antibacterial properties were synthesized with silver acetate as the metal source and 2-aminoterephthalic acid as the organic linker and were then embedded into thin-film composite (TFC) membranes to amend their performance as well as to alleviate biofouling. Silver metal−organic framework (Ag-MOF) nanorods with a length smaller than 40 nm were incorporated within the polyamide thin selective layer of the membranes during interfacial polymerization. The interaction of the synthesized nanorods with the polyamide was favored because of the presence of amine-containing functional groups on the nanorod's surface. The results of X-ray photoelectron spectroscopy, scanning electron microscopy, energy-dispersive X-ray spectroscopy, and atomic force microscopy characterizations proved the presence of Ag-MOF nanorods in the selective layer of thin-film nanocomposite (TFN) membranes. TFN membranes demonstrated improved water permeance, salt selectivity, and superior antibacterial properties. Specifically, the increased hydrophilicity and antibacterial potential of the TFN membranes led to a synergetic effect toward biofouling mitigation. The number of live bacteria attached to the surface of the neat TFC membrane decreased by more than 92% when a low amount of Ag-MOF nanorods (0.2 wt %) was applied. Following contact of the TFN membrane surface with *Escherichia coli* and *Staphylococcus aureus*, full inactivation, and degradation of bacteria cells were observed with microscopy, colony-forming unit tests, and disc inhibition zone analyses. This result translated to a negligible amount of the biofilm formed on the active layer. Indeed, the incorporation of Ag-MOF nanorods decreased the metal-ion release rate and therefore provided prolonged antibacterial performance.

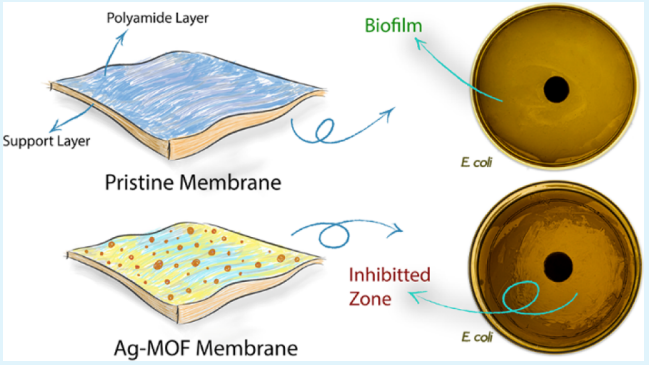

KEYWORDS: *forward osmosis, thin-film nanocomposite membranes, Ag-MOF nanorods, antibacterial activity, biofouling mitigation*

INTRODUCTION

Thin-film composite (TFC) polyamide membranes are widely applied in forward osmosis (FO) and desalination processes, as they currently provide the best combination of water flux and salt rejection.[1] However, the high susceptibility of polyamide-based membranes to biofouling, owing to their relatively high hydrophobicity, surface roughness, and the presence of carboxyl functional groups is the most significant challenge to the achievement of cost-effective operations of water desalination processes.[2,3] Because the surface properties dictate the interactions between foulants and the membrane, the vast majority of recent studies have focused on innovative strategies to prevent foulant attachment and to increase membrane lifespan.[4] Various approaches have been implemented, including physical surface coating, chemical functionalization, and *in situ* growth or incorporation of nanoparticles (NPs) within the polyamide layer.[5−7] Embedding NPs within the polyamide layer with the aim of fabricating thin-film nanocomposite (TFN) membranes presents specific advantages over other methods, including facile fabrication method and water flux enhancement.[8,9]

The embedment of NPs into the polyamide layer during the interfacial polymerization (IP) reaction is also a feasible method to obtain membranes with customized characteristics, such as fouling resistance.[10,11] The final performance of the

Received: July 20, 2020
Accepted: July 27, 2020
Published: July 27, 2020

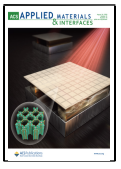

https://dx.doi.org/10.1021/acsami.0c13029
ACS Appl. Mater. Interfaces 2020, 12, 38285−38298

TFN membranes can be virtually tuned by designing NPs with specific properties and applying them during the IP procedure.[12,13] The first effort to fabricate TFN membranes for water treatment was reported in 2005 using zeolite-A as the nanofiller. Since then, diverse types of NPs, comprising carbon-based nanomaterials (*e.g.*, graphene oxide and carbon nanotube), minerals (*e.g.*, zeolite, titania, and silica), and metals or metal oxides (*e.g.*, silver, copper, and zinc oxide) have been utilized to develop TFN membranes. Despite significant advances in the fabrication of robust TFN membranes by effective incorporation of NPs into the polyamide layer, there are still bottlenecks that need to be tackled, including (i) the poor interaction of the NPs with the surrounding polyamide matrix, which increases the release of NPs during filtration and accordingly reduces their activity over time,[10,14] (ii) the inappropriate compatibility between the NPs and surrounding polyamide matrix, which adversely affects the membrane selectivity,[10] (iii) the improper size and morphology of NPs, which affect the polyamide selective layer mechanical strength and integrity,[15] (iv) the inhomogeneous dispersion of the NPs in the solution during the IP process and in the final polyamide layer, and (v) the difficulty of NPs synthesis and hence TFN membrane fabrication for large-scale applications.[16] Metal−organic frameworks[17] (MOFs) are among the most promising alternative materials proposed to address these bottlenecks.[18]

Because of the existence of the organic ligand in their structures, MOFs provide higher affinity and improved compatibility with the polyamide chain, in comparison to their fully inorganic counterparts. This greater interaction between the two components at the MOF−polymer interface can be related to covalent, hydrogen, and van der Waals bonds, which indeed prevent the formation of nonselective voids (*i.e.*, defects) between different phases.[10] Additionally, MOFs are widely reported for their antibacterial potential in the literature, as a source of metal centers with the potential for controlled release of biocidal agents.[19,20] The homogenous distribution of active metal centers in their frameworks offers a prolonged biocidal activity without aggregation or oxidation.[19] Despite being reported in the literature for the fabrication of the TFN membranes, few studies have achieved a suitable membrane functionalization without compromising membrane performance, and fewer have reported the biofouling behavior in the FO process.[21]

The main objectives of this study are (i) promoting interaction and compatibility between the polyamide matrix and the MOFs to improve their incorporation within the TFN membranes, (ii) improving surface hydrophilicity by incorporating Ag-MOF nanorods to minimize foulant deposition onto the membrane, (iii) introducing desirable charged moieties to exert electrostatic repulsion with biofoulants, and (iv) achieving high antibacterial activity and long-lasting anti-biofouling properties for TFN membranes with a simple approach. In this regard, we address the TFN membrane challenges by synthesizing and incorporating novel Ag-MOF nanorods with a length of 30−40 nm. Two approaches are investigated, whereby Ag-MOF nanorods are dispersed in the 1,3-phenylenediamine (MPD) aqueous solution or in the trimesoylchloride (TMC) organic phase during the IP reaction. The potential influence of Ag-MOF nanorods on the morphologies and surface hydrophilicity, as well as the chemistry of the TFN membranes are systematically investigated. The antifouling performance is evaluated by conducting fouling experiments using sodium alginate (SA) and *Escherichia coli* (*E. coli*) as model organic foulant and biofoulants, respectively. Finally, the antibacterial properties of the membrane are extensively studied *via* a combination of complementary techniques.

MATERIALS AND METHODS

Reagents. Polyethersulfone (PES, M_w = 58,000 g/mol, Ultrason E6020P) as the polymer, *N*,*N*-dimethylformamide (99.5%, Scharlau) as the solvent, and Triton X-100 (Merck) and polyvinylpyrrolidone (M_w = 25,000 g/mol, Merck) as pore formers were used for the preparation of the casting solutions to fabricate the support layer of FO membranes. TMC (Merck), MPD (Merck), triethylamine (TEA, Merck), camphorsulfonic acid (CSA, Merck), and *n*-hexane (99%, Scharlau) were used for the synthesis of the polyamide selective layer by IP reaction. Sodium chloride (NaCl, 99.5%, Merck) was used as a draw solute (DS) at different concentrations in FO filtration experiments. Silver acetate (≥98.0%, Merck) and 2-aminoterephthalic acid (NH_2-BDC, ≥95.0%, Sigma-Aldrich) were used for the synthesis of Ag-MOF nanorods. Potassium dihydrogen phosphate (KH_2PO_4, 99.5%), glucose monohydrate, magnesium sulfate ($MgSO_4{\cdot}6H_2O$, 99%), ammonium chloride (NH_4Cl, 99.5%), sodium bicarbonate ($NaHCO_3$, 99.5%), and calcium chloride ($CaCl_2$, 96%) were purchased from Merck for the preparation of synthetic wastewater feed solutions. SA was obtained from Sigma-Aldrich and used as a representative organic foulant.

Synthesis and Characterization of Ag-MOF Nanorods. A solution of silver acetate (0.2 g) in 100 mL of deionized (DI) water was gradually added to the NH_2-BDC solution (0.1 g dissolved in 100 mL of ethanol) while stirring slowly at 100 rpm, to form a precipitate after the synthesis reaction. Prior to the synthesis, both solutions were sonicated for 5 min to obtain homogenous solutions without any agglomeration. The final mixture was stirred for 30 min to complete the reaction, after which the precipitate was filtered and washed twice with 100 mL of ethanol to remove the unreacted reagents and then dried at 60 °C. The sample was then analyzed using Fourier transform infrared (FTIR) and energy-dispersive X-ray (EDX) spectroscopic analysis to confirm the successful formation of Ag-MOF nanorods. The morphology of Ag-MOF nanorods was observed using field-emission scanning electron microscopy (FESEM) (TESCAN MIRA3) equipped with an EDX spectrometer.

Preparation of the Neat TFC and the TFN Membranes. The PES support layer was fabricated *via* phase separation method induced by nonsolvent.[10] The TFC membranes were fabricated on the surface of the PES support layer through an IP reaction involving MPD aqueous and TMC organic solutions.[10] The TFC polyamide membrane (M0) was prepared by soaking the PES substrate in an aqueous solution containing 2 wt % MPD, 1 wt % TEA, and 2 wt % CSA for 2 min. An air-knife was then used to cautiously remove the excess MPD solution from the membrane surface. The amine-saturated membrane was then immersed in a 0.1 wt/v % TMC solution (*n*-hexane solvent) for 30 s. Subsequently, the membrane was placed inside a preheated oven at 80 °C for 5 min to complete the formation of the polyamide selective layer. The TFN membranes were fabricated by suspending Ag-MOF nanorods (0.2 wt %) into the aqueous MPD solution (M1) or into the organic TMC solution (M2) during the IP process. Before use, these solutions containing the Ag-MOF nanorods were sonicated for 20 min to prevent any undesired agglomeration. All the membranes were stored in DI water at 20 °C before testing or characterization.

Membrane Characterization. FESEM (MIRA3 TESCAN) equipped with an EDX detector was applied to characterize the surface and cross-sectional morphologies of the membranes. Atomic force microscopy (AFM, EasyScan II, Swiss) was used to determine the surface roughness of the membrane samples. To minimize the experimental error, the surface roughness was determined for three separately cast membranes. The surface chemistry of the membranes was studied by attenuated total reflectance−FTIR (ATR−FTIR, Thermo Scientific USA) and X-ray photoelectron spectroscopy (XPS, Bestec, Germany). The surface charge of both neat TFC (M0)

https://dx.doi.org/10.1021/acsami.0c13029
ACS Appl. Mater. Interfaces 2020, 12, 38285−38298

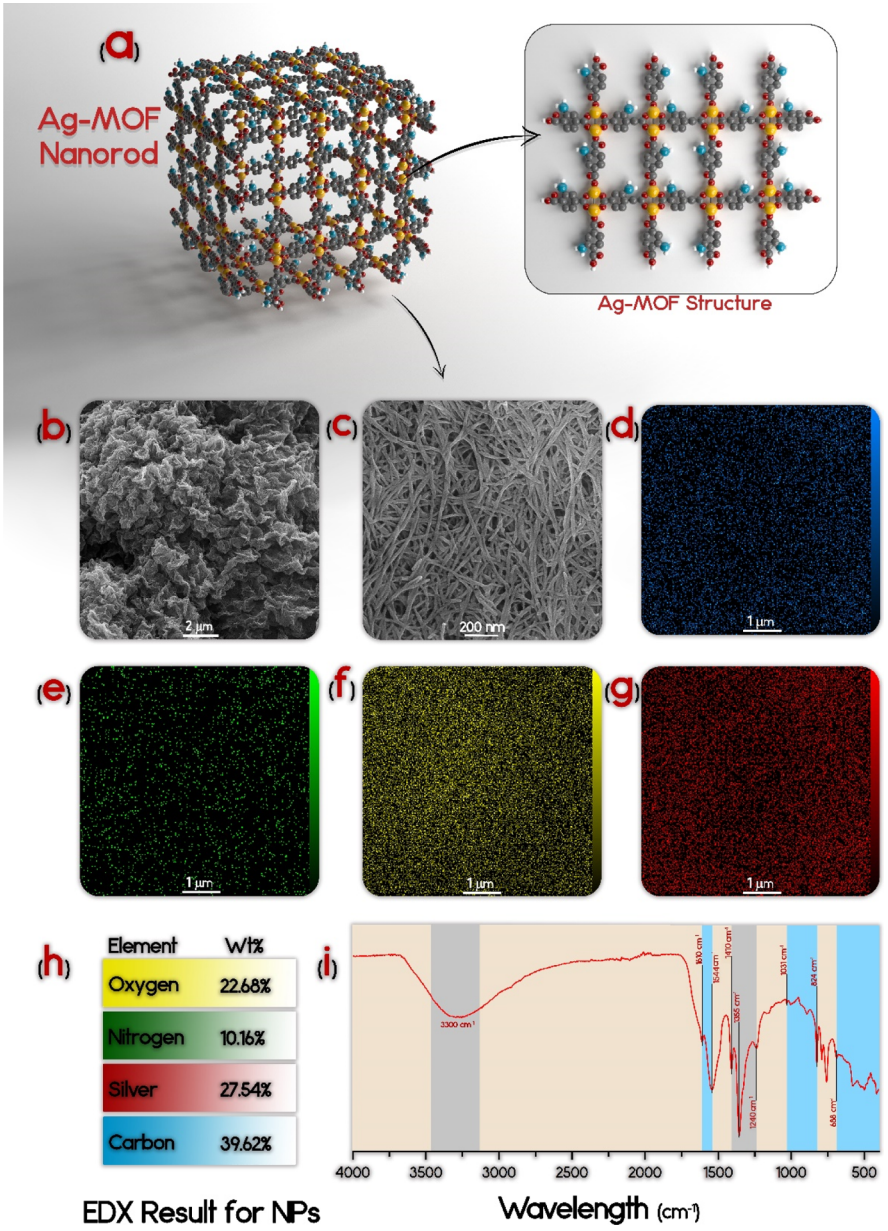

Figure 1. (a) Schematic illustration of the Ag-MOF structure (gray: carbon, yellow: silver, blue: nitrogen, white: hydrogen, red: oxygen); (b,c) representative FESEM micrographs of Ag-MOF nanorods; EDX mapping of (d) carbon, (e) nitrogen, (f) oxygen, and (g) silver on Ag-MOF nanorods; (h) elemental EDX composition of Ag-MOF nanorods; and (i) FTIR spectrum of the as-prepared Ag-MOF nanorods.

membrane, as well as M1 and M2 TFN membranes, was assessed with a SurPASS electrokinetic solid surface zeta potential analyzer (Anton Paar USA, Ashland, VA). All the streaming potential measurements were conducted in a background electrolyte solution composed of 1 mM KCl at 25 °C over a pH range 4−9. The zeta potentials of the membranes were computed based on the Helmholtz−Smoluchowski equation. Two separate samples of each membrane were assessed to minimize the experimental error. The membrane surface hydrophilicity was assessed using contact angle measurements (Data-Physics, OCA 15 plus), where an average value was determined from measurements at five random positions. The elemental composition and chemical structure information of the membrane surface were evaluated by inductively coupled plasma−optical emission spectrometry (ICP−OES, Varian 730-ES), respectively. The silver-ion release rate from the membrane was determined by first storing 6.45 cm^2 coupons in 20 mL of DI water overnight under mild shaking, followed by acidifying the coupons with a 1% nitric acid solution and then shaking the samples at 100 rpm for 30 days. Water samples were withdrawn after 1, 7, 15, and 30 days, and the concentration of the released silver ions was determined using ICP−OES.

Evaluation of the Membrane Permeation Properties. The transport properties of all the membranes were assessed in terms of the water permeability coefficient (A) and salt permeability coefficient (B) with a cross-flow filtration setup with an effective membrane active area of 30 cm^2.[10] In FO filtration experiments, DI water was used as feed and NaCl as draw solutions, respectively. Further information on the FO unit and the performance assessment procedure are reported in Supporting Information (SI.1.1).[22]

Dynamic Fouling Experiments. The organic fouling and biofouling propensity of the FO membranes were assessed by adding SA (a model polysaccharide) and *E. coli* (model bacteria), respectively, in the feed solutions during FO filtration experiments. Further explanation on the fouling experiments are provided in the Supporting Information (SI.1.2).[10,23]

Fluorescent Scanning Microscopy. For epifluorescence microscopy, *E. coli* bacteria was used. Epifluorescence scheme was used for

https://dx.doi.org/10.1021/acsami.0c13029
ACS Appl. Mater. Interfaces 2020, 12, 38285−38298

the fluorescence imaging. In each experiment, 1 mL of the stock bacterial suspension was placed onto a 1 × 1 cm^2 membrane sample; viability staining was performed after 1 h of contact. The SYTO 9-stained bacteria (green) and PI-stained bacteria (red) corresponded to live and the dead cells, respectively. Further details on the fluorescence imaging procedures are presented in Supporting Information (SI.1.3).

Heterotrophic Plate Count. The *E. coli* bacteria, as a model Gram-negative bacteria, were grown at 37 °C in trypticase soy broth (TSB) with incubation and shaking overnight. After this period, a fresh broth sample was incubated with some of the bacterial TSB suspension for 3 h at 37 °C. By centrifuging for 2 min at 6000 rpm, the bacterial culture was then fully pelletized. The resulting bacterial solution was suspended again in 1× sterile phosphate buffer saline (PBS) solution to achieve a final concentration of 10^7 cfu/mL. Membrane samples with a surface area of a 4 cm^2 were incubated at 37 °C in a sterile Petri dish containing the bacterial solution under continuous mild shaking for 1 h. The unattached bacterial cells were removed by rinsing the membrane samples three times with a PBS solution. Upon resuspending the attached bacteria, membrane samples were then placed in a sterile plastic bag with 10 mL of PBS stock solution and then sonicated for 7 min. The resulting solution was transferred to previously prepared TSB agar plates after series dilutions; the plates were finally incubated for 24 h at 37 °C, and the CFU was finally counted.[24]

Heterotrophic plate count-*Staphylococcus aureus* (*S. aureus*), as a model Gram-positive bacteria, was tested for investigating the antibacterial properties of the synthesized membranes. The *S. aureus* was cultured in the TSB overnight by shaking and incubating at 37 °C. The overnight culture was mixed with some freshly prepared TSB and were incubated for 3 h. The culture was centrifuged at 6000 rpm for 3 min and was resuspended in 1× PBS to attain a final concentration of 10^5 cfu/mL; 1 mL of this bacterial solution was exposed to the 1 × 1 cm^2 of the active surfaces of the membranes. The membranes with the bacterial solution was incubated for 1 h with proper shaking. The membranes were then washed with 10 mL of sterile PBS solution, and this was plated on trypticase soy agar (TSA) plates overnight at 37 °C for determining the viability of the unattached cells; the number of cells were counted in terms of CFU.

Disc Inhibition Zone Assay. To further explore the antibacterial activities of the membranes, a disc inhibition zone test was performed to determine the inhibition zone of all the membranes.[25] TSB (5 mL) was poured inside Petri dishes and solidified in a biosafety cabinet. The plates were incubated at 37 °C for 24 h to eliminate any plates with contamination. *E. coli* fresh suspensions were obtained as described above. A sterile cotton swab was then dipped into the *E. coli* suspension and was spread on the agar plates. The membranes were cut into 6 mm diameter discs, which were placed in the middle of the agar plates already inoculated with *E. coli*. The plates were then incubated (without shaking) for 24 h at 37 °C. For the *S. aureus* inhibition zone test, an overnight-grown *S. aureus* liquid culture was smeared evenly with a sterile cotton swab on the top of TSA plates and the disc cut from each membranes were placed aseptically in the middle of each plates. After stationary overnight incubation at 37 °C, the inhibition zone for each disc was determined. A negative control without any disc on the plate was also included to monitor contamination and die-off.

RESULTS AND DISCUSSION

Characteristics of Ag-MOF Nanorods and Proposed Interaction with Polyamide. Figure 1a illustrates the schematic structure of Ag-MOF nanorods. To confirm the successful synthesis of the nanorods, a thorough morphological and physicochemical characterization was conducted. As illustrated in Figure 1b,c, the FESEM micrographs of the as-prepared Ag-MOF samples demonstrated the narrow size distribution of nanorods within the range of 30−40 nm. Figure 1d−g presents EDX mapping of carbon, nitrogen, oxygen, and silver atoms on Ag-MOF nanorods. The elemental EDX composition of Ag-MOF nanorods (Figure 1h) indicated 27.54 and 10.16% of silver and nitrogen, respectively. The infrared absorption peaks observed in the IR spectrum of Figure 1i can be summarized as follows: the broad peak centered around 3300 cm^{-1} is the fingerprint for O−H stretching.[26] The observed peak at 1544 cm^{-1} is attributed to C−N stretching and also N−H bending.[18,27] Additionally, N−H stretching is observed at 1610 cm^{-1}.[27] The two peaks identified at 1355 and 1410 cm^{-1} most likely correspond to C═C and C═O stretching, respectively. The peak at 1240 cm^{-1} is because of C−O−C symmetric stretching.[28] Moreover, the peak at 1031 cm^{-1} is related to C−O stretching.[29,30] Besides, several peaks observed in the range of 824−688 cm^{-1} may be assigned to C−H bonding, especially rocking vibrations.[28,30] The more subtle peaks between 500 and 577 cm^{-1} can be associated with Ag−O vibrations.[31]

As with all other nanomaterials, incorporation of MOFs influences the polyamide-based layer structure, as nanostructures may change the kinetics of IP reaction, interact with the polyamide matrix, and may alter the degree of acid chloride hydrolysis.[32] Indeed, the penetration rate of MPD/TMC monomers into the reaction zone may alter during the IP process, and usually, a looser polyamide layer forms. In this study, both the aqueous MPD and the organic TMC solutions underwent a color change upon the introduction of the Ag-MOF nanorods, which was more intense in the case of MPD solution, whereby its color turned rapidly from transparent to black.[33] The amine functional groups existing on the surface of Ag-MOF nanorods most likely interacted with MPD and/or TMC molecules before and during the IP process, thus influencing the degree of the polycondensation reaction mediated by amine and acyl chloride monomers and therefore the final polyamide structure. The amino groups of Ag-MOF nanorods can form covalent bonds with TMC monomers, whereas they interact with diamine-containing MPD monomers *via* hydrogen bonds. Both types of interactions improved the dispersion and compatibility of MOFs in the polyamide matrix.[34,35] Figure 2 presents a schematic of possible interaction between Ag-MOF nanorods and the polyamide chains during the IP process. A further schematic of the aqueous MPD and organic TMC solutions immediately after the introduction of Ag-MOF nanorods at ambient temperature is presented in Supporting Information (Figure S1).

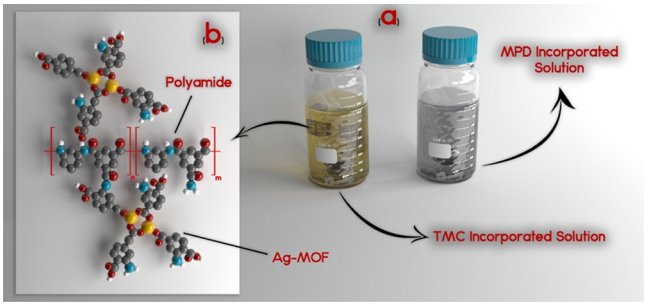

Figure 2. (a) Graphic illustration of the aqueous MPD and organic TMC solutions immediately after addition of Ag-MOF nanorods; (b) proposed mechanism of interaction between the Ag-MOF nanorods and the polyamide matrix in which the active sites of both hydrogen and covalent bonds are defined (yellow: silver; gray: carbon; blue: nitrogen; red: oxygen; white: hydrogen).

https://dx.doi.org/10.1021/acsami.0c13029
ACS Appl. Mater. Interfaces 2020, 12, 38285−38298

To study the membrane surface functional groups and to further validate the successful binding of Ag-MOF nanorods (Figure 3), ATR−FTIR spectroscopy was applied. The broad

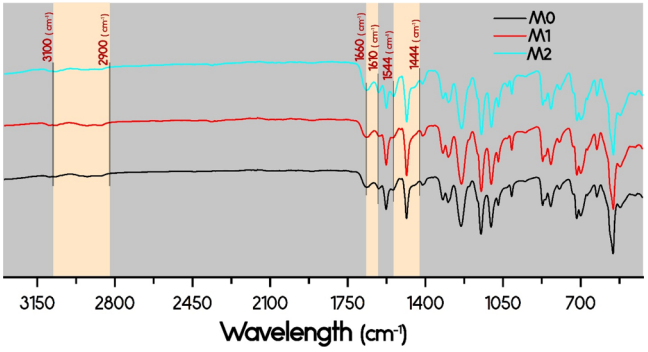

Figure 3. ATR−FTIR spectra of the neat M0 and the nanocomposite M1 and M2 membranes.

peak around 3300 cm^{-1} represents the O−H stretching.[26] The peaks over the wavenumbers of 1150−1320 cm^{-1} are related to PES support and are detected in all membranes.[36] The peaks identified at 1150 cm^{-1} can be ascribed to the stretching vibrations of symmetric O═S═O of the sulfone functional groups. The peaks observed around 1300 and 1320 cm^{-1} corresponded to the doublet from the stretching vibrations of asymmetric O═S═O and 1240 cm^{-1} to the stretching vibrations of asymmetric C−O−C of the aryl ether group of the PES sublayer, respectively.[37] The inherent peaks of the polyamide layer formed *via* the IP process are observed at around 1660 cm^{-1} (C═O stretching vibrations of amide I), at about 1544 cm^{-1} (stretching vibrations of in plane N−H bending and C−N of amide II), and 1610 cm^{-1} (stretching of the amide's N−H).[27] The appearance of the peak at 1444 cm^{-1} is attributed to C═O vibration of carboxylic acids,[26] possibly emanated from the free carboxyl functions of NH_2-BDC linker or the hydrolysis of unreacted acyl-chloride functional groups.[27] Moreover, the significant increment of N−H bending vibration at 1544 cm^{-1} can be assigned to the NH_2-BDC linker, which indicates the presence of Ag-MOF nanorods.

Characteristics of TFC Membranes. XPS was performed to investigate the elemental structure and chemical bonds of the neat M0, and the M1 and M2 TFN membranes. As shown in Figure 4, the energy spectra of all membranes mainly involved carbon (C), oxygen (O), and nitrogen (N) peaks, which were located at binding energies of 285 eV (assigned to C 1s), 400 eV (N 1s), and 531 eV (O 1s).[22,38] The appearance of two new silver peaks at about 368 eV and 374 eV (attributing to Ag $3d_{5/2}$ and $3d_{3/2}$, respectively)[39] suggests the presence of Ag-MOF nanorods in the structure of TFN membranes. It must be noted that no silver signal was observed

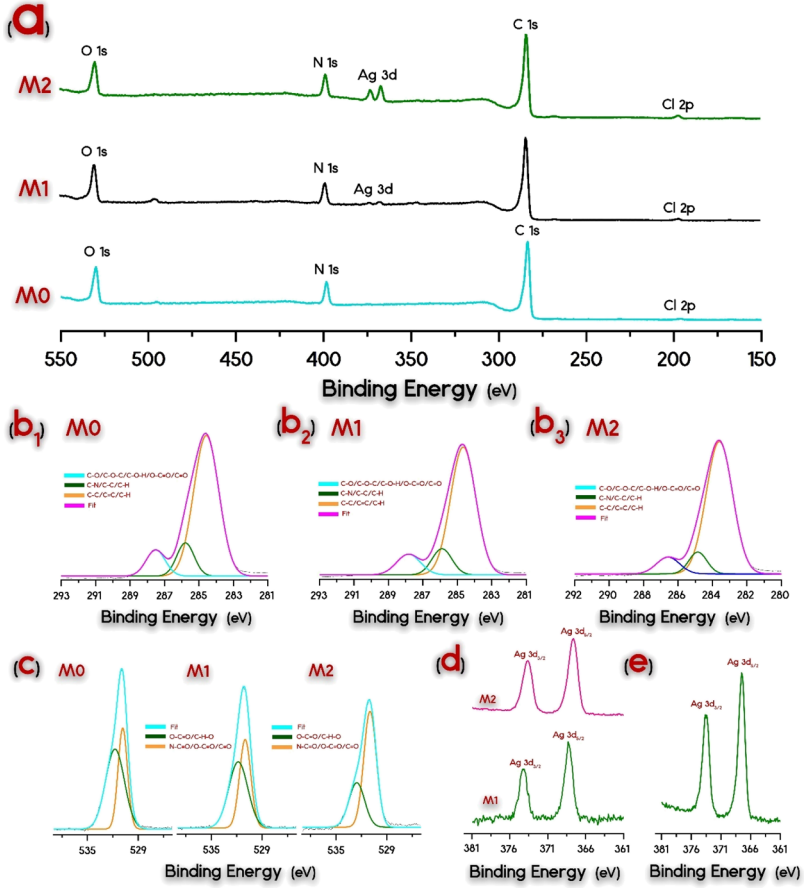

Figure 4. (a) XPS survey spectra of the neat M0 and of the M1 and M2 TFN membranes: deconvoluted high-resolution C (1s) spectra of (b_1) the neat M0, (b_2) M1, (b_3) and M2 TFN membranes; (c) deconvoluted high-resolution O (1s) spectra of the neat M0, and of the M1 and M2 TFN membranes; (d) deconvoluted high-resolution Ag spectra for M1 and M2 samples; and (e) intensity ratio of Ag 3d spectra between M2 and M1 membranes.

https://dx.doi.org/10.1021/acsami.0c13029
ACS Appl. Mater. Interfaces 2020, 12, 38285−38298

in the survey spectra of the neat M0 membrane (Figure 4a). Gaussian function was used for peak fitting. In the case of high-resolution C 1s spectra (Figure 2b), three peaks can be identified: a major peak approximately at 285 eV,[40] mostly attributed to the carbon atoms in benzene ring correlated to C−H, C−C, and C−C bonds;[41,42] an intermediate peak at 287 eV assigned to C−N, C−O, and C−O−C bonds;[43] and also a minor peak approximately at 288 eV attributed to O−C−O and amide O═C−N bonds.[22,38,42] High-resolution O 1s spectra are instead best fitted by two peaks, whereby the major peak is located at about 532.5 eV, attributed to C═O (O−C−O, N−C−O, and C−O bonds), and the minor peak is located around 533.5 eV related to C−O (C−O−H and O−C−O bonds).[22,44,45]

The elemental compositions of all the membranes are reported in Table 1. Theoretically, the O/N ratio of polyamide varies between the value of 1 for a fully cross-linked structure and 2 for a fully linear structure.[46] A greater degree of crosslinking reflects a denser polyamide layer with increased selectivity, while a lower degree offers improved hydrophilicity and higher permeability. The results of the elemental compositions (Table 1) indicate that the Ag-MOF incorporation increased the O/N ratio for M1 and M2 membranes, compared to that of the M0 membrane. This in turn can be interpreted as a lower cross-linking degree of the polyamide structure.

Table 1. Elemental Compositions, O/N Ratio, and Ag Spectra Intensity Ratio of the Membranes

	atomic concentration (%)					
membrane	C (1s)	O (1s)	N (1s)	Ag (3d)	O/N ratio	M2/M1 Ag ratio (from spectra intensity)
M0	60.0	23.2	16.1	0.0	1.48	
M1	59.7	25.7	12.5	2.0	2.05	
M2	56.7	19.7	11.5	12.1	1.71	6.05

On the other hand, what stands out in Figure 4e is that the intensity ratio of the XPS spectra related to silver for M2 and M1, (M2/M1), was about 6:1, indicating that the M2 sample contained more Ag on the outermost layer despite adding the same amount of MOFs to the solutions during preparation. A likely explanation is that the IP reaction is primarily governed by the diffusion of MPD molecules into the reaction region; therefore, the polymer film develops in a direction from the interface toward the organic solution,[36] thus entrapping more MOFs into the topmost polyamide layer (for M2 fabrication, nanorods were added to the organic TMC solution). Considering that the penetration depth of the X-ray in XPS analysis is generally less than 10 nm of the top selective layer,[47] the results are rationalized with a higher Ag-MOF concentration near the topmost surface of M2 membranes, translating into a potentially higher content of Ag ions accessible to the surface.[48] Figure 5 illustrates the relevant EDX mapping and EDX elemental composition of M1 (Figure 5d) and M2 (Figure 5h) nanocomposite membranes, clearly corroborating the presence of Ag atoms. It should be noted that the EDX analysis covers the entire thickness of sample, while XPS analysis covers roughly the uppermost portion of the selective layer. The Ag detected by EDX was almost identical for both M1 and M2 membranes. This result suggest that, while the same amount of Ag-MOF was incorporated in the two membranes, the nanorods preferentially accumulated near the topmost surface of M2 membrane selective layers.

The surface and cross-section micrographs of the neat TFC and TFN membranes are presented in Figure 6. The neat M0 membrane (Figure 6a,b) displayed a ridge and valley surface, which is the typical morphology of polyamide TFC membranes fabricated by the IP reaction.[49] Although no obvious change occurred in the top surface morphology of nanocomposite membranes, bright spots appeared on their surface upon the incorporation of Ag-MOF nanorods in the layer. These features can be attributed to the presence of Ag atoms within the core of Ag-MOF nanorods. Such spots are more easily observed in the cross-sectional images, with a uniform distribution throughout the thickness of the M2 TFN sample (Figure 6h,i). Because the sensitivity of heavy elements, such as silver, to the backscatter electrons is significantly higher than that of light ones, such as carbon, nitrogen, and oxygen,[50] a backscattered imaging detector was applied to identify and

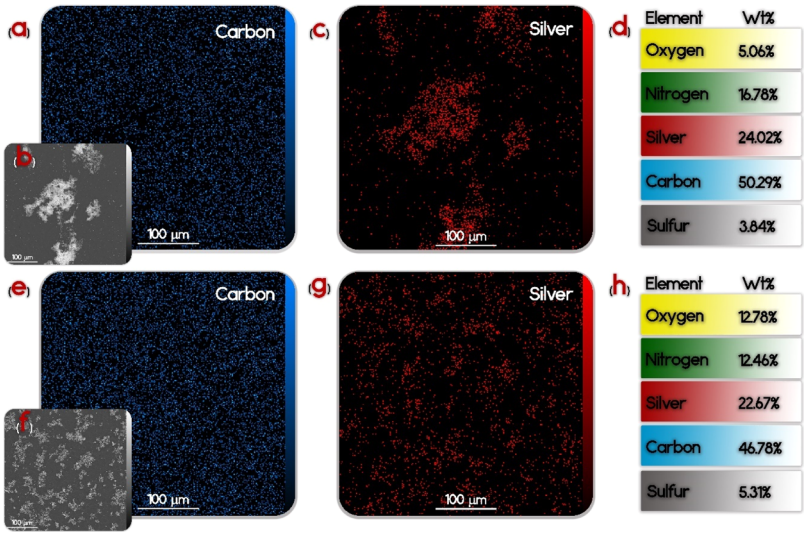

Figure 5. EDX analyses for (a−d) M1 membrane and (e−h) M2 membrane. (a,e) EDX mapping of carbon; (b,f) surface FESEM images; (c,g) EDX mapping of silver; and (d,h) EDX elemental compositions.

https://dx.doi.org/10.1021/acsami.0c13029
ACS Appl. Mater. Interfaces 2020, 12, 38285−38298

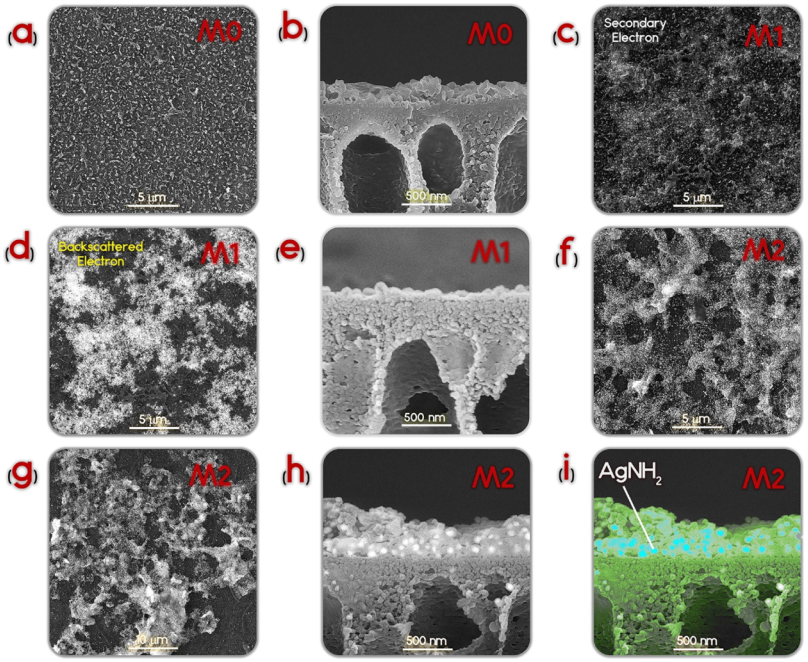

Figure 6. (a) Surface and (b) cross-section FESEM micrographs of the neat M0 membrane; (c) surface in the secondary mode, (d) surface in the backscatter mode, and (e) cross-section FESEM micrographs of the M1 membrane; and (f,g) M2 membrane surface in the backscatter mode, and (h) cross-sectional and (i) colored cross-sectional SEM of the M2 membrane.

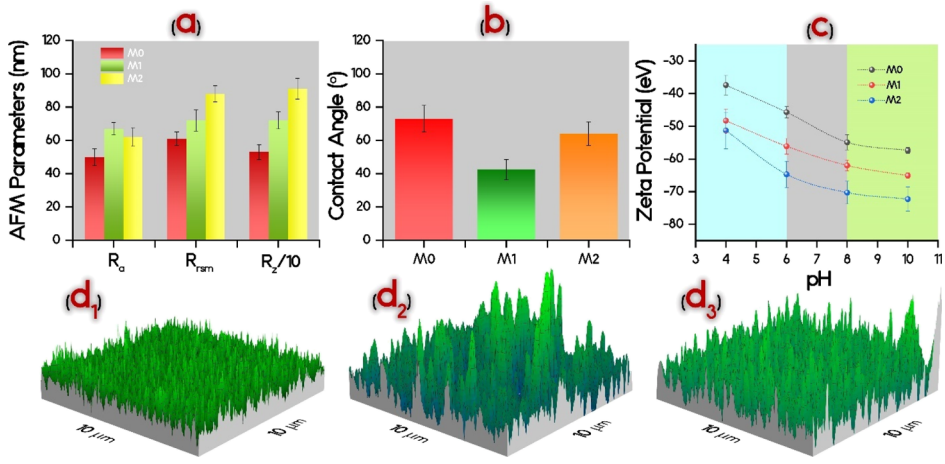

Figure 7. (a) AFM roughness parameters; (b) contact angles; (c) zeta potential; and representative AFM images of (d_1) M0, (d_2) M1, and (d_3) M2 membranes.

isolate the heavy elements (see Figures S2−S4). These small spots were uniformly distributed within the M1 and M2 TFN layers, whereas such bright spots were not detected while imaging the neat M0 membrane. These results may be interpreted with high density and rather homogenous dispersion of the Ag-MOF nanorods within the polyamide layer of TFN membranes, corroborating the hypothesis that there is suitable compatibility between the two phases represented by nanorods and the polyamide matrix.[51] Moreover, the cross-sectional morphology of the M1 membrane shows that, by loading the aqueous MPD solution with Ag-MOF during IP, the average thickness of the TFN layer decreased.[52] Indeed, the incorporation of the nanorods may thwart the MPD diffusion into the organic solution during polymerization and delay the formation of the polyamide film because of the steric hindrance of Ag-MOF.[53] This decrement in layer thickness would diminish the mass transfer resistance and eventually result in improved water flux.[54]

More morphological features were observed using AFM, and the results are summarized in Figure 7a (roughness parameters) and Figure 7d_1−d_3 (three-dimensional AFM images, see Figure S5). The roughness parameters were higher for membranes fabricated by incorporation of Ag-MOF nanorods, consistent with results from SEM observations, which suggested the formation of additional features within the polyamide because of the presence of Ag-containing nanorods. This result is especially true for M2 membranes, which showed significantly larger values of root-mean-square and R_z roughness. This observation may again stem from the different fabrication procedure. During the preparation of M2, nanorods are dispersed in the TMC solution, and their amount near the organic/water interface is probably higher in comparison with the protocol to prepare the M1 membrane, where only the

https://dx.doi.org/10.1021/acsami.0c13029
ACS Appl. Mater. Interfaces 2020, 12, 38285−38298

Table 2. Transport Properties of the Neat TFC and TFN Membranes

membrane	A	B	B/A	S	$R^2(J_w)^a$	$R^2(J_s)^b$
M0	1.10 ± 0.1	0.335 ± 0.02	0.34 ± 0.01	123 ± 1	0.98 ± 0.02	0.95 ± 0.1
M1	2.24 ± 0.1	0.410 ± 0.02	0.293 ± 0.01	206 ± 1	0.975 ± 0.01	0.879 ± 0.1
M2	1.49 ± 0.1	0.366 ± 0.02	0.245 ± 0.01	279 ± 1	0.907 ± 0.01	0.924 ± 0.1

$^a R^2(J_w)$: water flux coefficient of determination. $^b R^2(J_s)$: solute flux coefficient of determination.

pores of the support are soaked with the nanorod-containing MPD solution. Overall, from SEM, XPS, and AFM results, it can be concluded that dispersing nanomaterials in the organic solution (M2 membrane) results in a thicker and rougher selective film, with a higher density of Ag-MOF nanorods embedded in the topmost portion of this layer. It has been reported that rougher membranes are generally more prone to biofouling by bacterial cells and macromolecules. However, a complex relationship exists between roughness, hydrophilicity, and fouling behavior, which cannot be solely rationalized from the surface morphological analysis.[55]

To obtain information on the surface hydrophilicity, the average water contact angle of the membranes was measured and the results are showed in Figure 7b. The average contact angle reduced from 72.6 ± 5.1° for the neat M0 membrane to 43.4 ± 3.1 and 63.2 ± 2.8° for M1 and M2 samples, respectively. This increase in the membrane wettability probably emanates from the presence of hydrophilic Ag-MOF nanorods, which contain numerous functional groups on their surface that have a tendency to form hydrogen bonds with water molecules. Although larger roughness was observed for the nanocomposite membranes, the role of surface chemistry often offsets that of surface roughness in the rate of fouling during membrane filtration.[55] The likelihood of the hydrogen bond between the membrane surface and the surrounding water molecules promotes the formation of a thin layer of water at the membrane surface/liquid interface, which prevents bacteria deposition and alleviates the undesirable attachment of hydrophobic foulants in general.[56]

The surface charge is also a crucial factor when it comes to treating a feed solution with charged foulants.[57,58] A negatively charged membrane typically shows a lower propensity to biofouling by bacterial cells, which carry a net negative charge in the pH range 4−9, through electrostatic repulsion.[59] Figure 7c reports the results of zeta potential for the membranes as a function of pH. The results are in agreement with the protonation behavior of polyamide carboxyl groups deprotonating at increased pH values, thus imparting an overall negative potential to the surface.[60] What is interesting in the data presented in Figure 7c is the larger values of negative zeta potential of both M1 and M2 nanocomposite membranes compared to traditional polyamide membranes. This result may be related to the additional contribution of the free carboxylic groups present in the framework of Ag-MOF nanorods. M2 membranes showed the largest negative charge among the membranes, which may again be attributed to the higher density of Ag-MOF nanorods at the surface. This increased negative surface potential of both nanocomposite membranes may eventually result in reduced biofouling.[61]

Membrane Transport Properties. The transport parameters of the membranes were calculated based on a four-step FO procedure,[62] and the results are listed in Table 2 and illustrated in Figure 8. The results in terms of water flux, reverse salt flux, and water to reverse salt flux ratio are presented in Figure 8. The results indicate that J_w of the M1 membrane was higher while that of the M2 membrane was less than the water flux attained for the pristine M0 membrane. Furthermore, J_s of both M1 and M2 membranes was considerably smaller in comparison to M0 membranes. Overall, the specific solute flux (J_s/J_w) is a key membrane performance parameter, which should be low to allow high selectivity in the FO process. As presented in Figure 8c, both M1 and M2 TFN membranes showed lower J_s/J_w ratio [higher (J_w/J_s)] compared to M0. Nonetheless, this difference was less marked for M2 because of a lower value of water flux obtained with this membrane, which can be rationalized with the increased thickness of its selective layer, as suggested by FESEM micrographs.

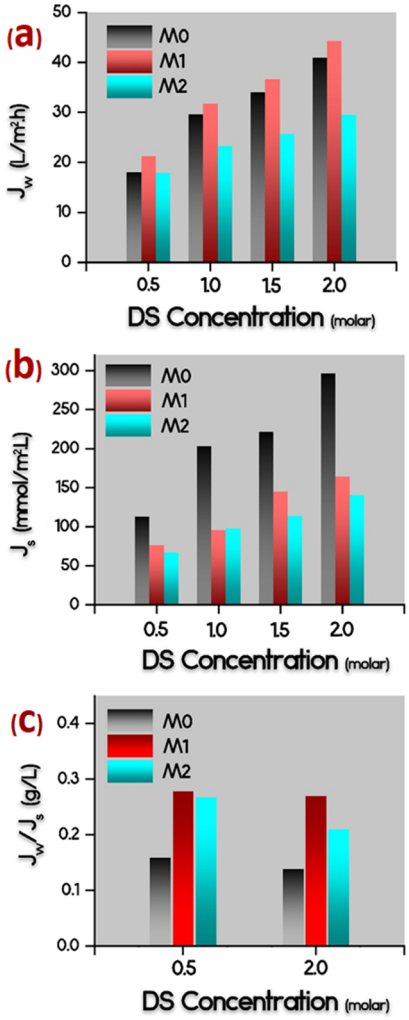

Figure 8. (a) Water flux, (b) salt flux, and (c) water over solute flux fraction *vs* the molar concentration of the NaCl draw solution.

From the data shown in Figure 8, the inherent transport characteristics of the polyamide or nanocomposite polyamide layers can be calculated (Table 2). Surprisingly, the water permeability coefficient, A, showed an increment from 1.1 to

https://dx.doi.org/10.1021/acsami.0c13029
ACS Appl. Mater. Interfaces 2020, 12, 38285−38298

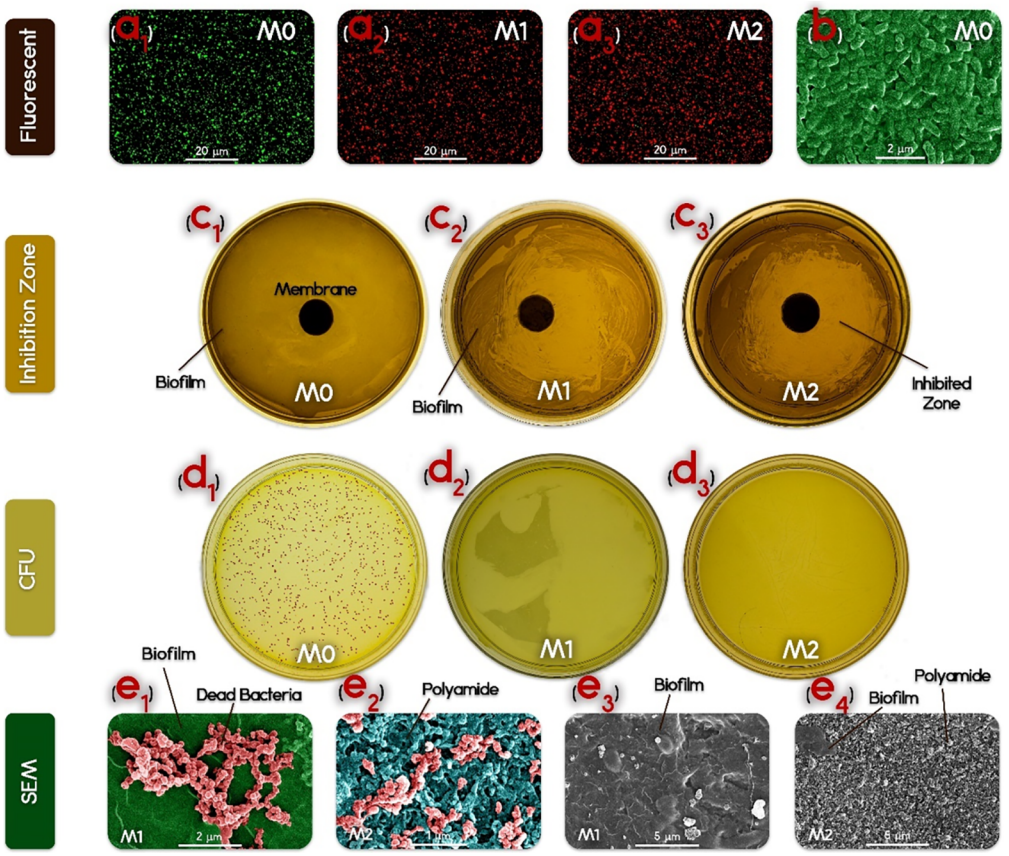

Figure 9. Antibacterial properties of the membranes. Fluorescent photographs of *E. coli* cells accumulated to the surface of (a_1−a_3) neat M0, M1, and M2 membranes, respectively; stained by SYTO 9 (green) and PI (red) for viable and dead cells, respectively; (b) SEM images of live bacteria attached to the surface of the M0 membrane; disc inhibition zone test results obtained with (c_1−c_3) neat M0, M1, and M2 membranes, respectively; CFU's from plating bacterial suspension previously in contact with (d_1−d_3) neat M0, M1, and M2 membranes, respectively; (e_1−e_4) SEM images of the bacterial cells attached to the surface M1 and M2 membranes.

2.24 L m^{-2} h^{-1} bar^{-1}, while the *B* value enhanced only slightly, from 0.33 to 0.41 L m^{-2} h^{-1} when nanorods were introduced into the layer to form M1 membranes. The same trend but of lower magnitude was observed for the M2 membranes. Therefore, the ratio of salt permeability/water permeability (*B*/*A* ratio) decreased when membranes were synthesized by incorporating Ag-MOF nanorods within the polyamide layer, suggesting the enhanced performance of the nanocomposite membranes. The lower the *B*/*A* ratio, the more enhanced the selectivity and the sustainability of the FO process.[63,64] The improved transport properties may be related to the increased hydrophilicity compared to the conventional polyamide membrane. Another reason for the enhanced permeation properties of nanocomposite membranes can be the formation of nanosized voids at the interface of MOFs and polyamide matrix. Normally, inhomogeneous distribution of NPs in the top polyamide layer because of their aggregation and weak compatibility with the polymer are two limiting features that adversely affect the performance of the TFN membrane.[65] As the thickness of the polyamide selective layer falls in the range of 100−300 nm, nanomaterials must have a significantly smaller size of at most tens of nanometers to prevent defect formation, which would translate into compromised salt selectivity. In the present work, although Ag-MOF nanorods offered improved compatibility with the polyamide matrix, some gaps may still form between polymeric chains during the IP reaction. These gaps would increase the void fractional volume and provide more facile transport of both water and salt molecules. However, in this study, the influence of these voids on the transport of water seemed overwhelming compared to that on salt, leading to enhanced overall performance.[66]

Antibacterial Properties of the Membranes. The antibacterial properties of the membranes were first evaluated by viable and dead staining and detected by fluorescence microscopy with *E. coli* and *S. aureus* as model Gram-negative and Gram-positive bacteria, respectively. Figure 9a_1−a_3 report representative fluorescent photographs of the *E. coli* bacteria accumulated to the membranes after incubation in the bacterial suspension. Nearly all bacteria on the conventional TFC membrane surface were alive following incubation; in contrast, the number of live bacteria remaining on the surface of TFN membranes was reduced substantially. Mortality rates of approximately 90 and 96% were observed following incubation with the M1 and M2 TFN membranes, respectively. Notably, these high bacterial inactivation rates were obtained by loading a low concentration of the nanorods (0.2% by mass).[67] The disc inhibition zone method also illustrated that contact with the membrane surface inhibited biofilm growth on the plate (Figure 9c_1−c_3). Specifically, no inhibition zone for the M0 membrane was observed, while there was an evident inhibition zone for both M1 and M2 membranes.

The CFU experiments (Figure 9d_1−d_3), in which unattached cells were plated after the biological suspensions

https://dx.doi.org/10.1021/acsami.0c13029
ACS Appl. Mater. Interfaces 2020, 12, 38285−38298

were exposed to the membrane also suggested a strong biocidal effect for both M1 and M2 membranes. Almost no viable cells were visible after contact with M1 and M2, as opposed to M0, on which many marked colonies formed instead. Finally, SEM images (Figure 9b,e_1−e_4) showed healthy *E. coli* cells (Figure 9b) on the M0 membrane and degraded *E. coli* cells on M1 (Figure 9e_1,e_3) and M2 membranes (Figure 9e_2,e_4), consistent with the results discussed above. Taking a closer look at SEM images, a uniform biofilm is visible on M1 which consisted of bacteria whose structure was clearly compromised, while a little biofilm was formed on M2 membranes. The same trend observed for *E. coli* was detected for *S. aureus* which showed no antibacterial activity for the M0 membrane (Figure S6). The disc inhibition zone test and cfu experiments determined that membranes M1 and M2 were highly antibacterial against *S. aureus*.

The results summarized in Figure 9 suggest high antibacterial properties of the nanocomposite membranes against Gram-negative bacteria. The high inactivation rate observed in this study was accomplished after a short contact time between the bacteria and the membrane (1 h); generally, a longer incubation time (greater than 2 h) has been reported to obtain such behavior.[68] This observation indicates that, despite being mostly buried within a polyamide layer, Ag-MOF nanorods are still active and can trigger bacterial inactivation at the membrane surface. MOFs can act as reservoirs of Ag^+ ions, whereby the gradual leakage of the metal center to the surrounding environment is the most probable cause for the toxicity of MOFs.[18,69−71] The content of antibacterial cations in Ag-MOF nanorods is relatively high.[70−72] The Ag active sites in the structure of Ag-MOF nanorods are uniformly distributed, and the release mechanism of Ag ions should not change during the degradation of the framework. Because the antibacterial activity is directly related to the release of Ag^+ ions,[71] the greater the number of released ions, the higher the inactivation rates. The concurrent gradual release of the organic linker present in the MOF structure may result in a synergetic antibacterial property.[19,69,73] While the most probable antibacterial mechanism is related to the release of Ag^+, other possible antibacterial mechanisms proposed for Ag-MOF biocidal properties are (i) direct attachment to bacterial cells, infiltration, and physical destruction of the cell membrane and (ii) indirect generation of reactive oxygen species which trigger damage to the bacteria cell structure.[74] Overall, it is desirable to locate the Ag-containing nanomaterials as much as possible near the membrane surface, where maximum interaction and direct contact with the bacteria can be attained. In this study, Ag-MOF nanorods with small size were homogenously distributed within the TFN membrane active layer and this resulted in successful inhibition of biofilm formation. The Ag-MOF nanorods were immobilized with higher density near the surface of the nanocomposite layer of the M2 membrane (as discussed in Figures 5 and 6). This configuration may be responsible for the higher antibacterial activity of M2.

Dynamic Organic Fouling and Biofouling Evaluation. The evaluation of flux decline because of organic fouling was performed by SA (as representative organic foulant) in the FO filtration mode and the results are provided in Figure 10a. Prior to each fouling or biofouling experiment, a baseline experiment was performed to eradicate the impact of draw solution dilution and reverse salt diffusion. The nanocomposite membranes demonstrated reduced flux decline and higher flux

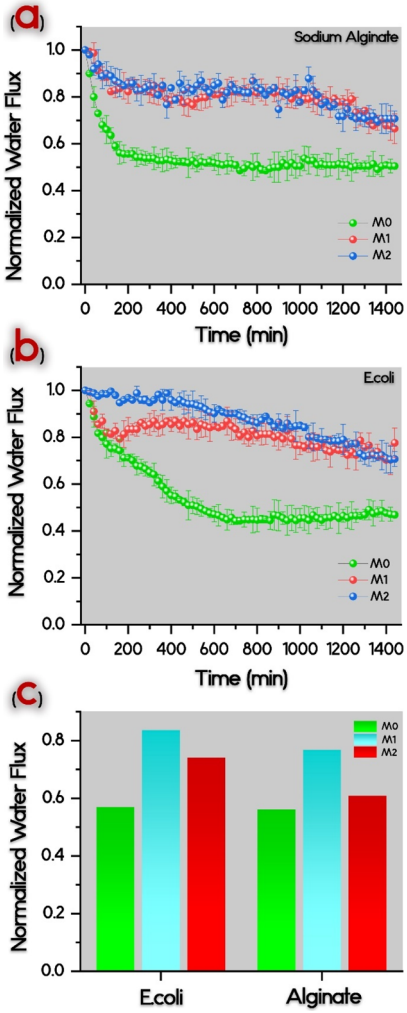

Figure 10. Results of fouling experiments under FO filtration using 1 M NaCl as DS: (a) organic fouling conducted by SA; (b) biofouling conducted by *E. coli* (the standard deviation of three runs with fresh membrane samples); and (c) relevant water flux recovery ratios.

recovery ratio compared to M0 samples. This antifouling property can be related to the more hydrophilic nature of the surface of Ag-MOF-incorporated TFN membranes.[75] To investigate the impact of Ag-MOF nanorods on biofouling, filtration experiments were also conducted using a synthetic wastewater feed containing *E. coli*. The results from biofouling experiments are presented in Figure 10b. Also, in this case, the performance of the nanocomposite membrane were remarkably better than that of the conventional membrane in terms of both reduced flux decline and improved flux recovery ratio. In this case, the improvement in performance can be attributed both to higher hydrophilicity, translating into lower bacterial deposition probability, and to the significant antibacterial activity of Ag-MOF nanorods, which in turn prevented biofilm proliferation. Although the M2 membrane provided higher antibacterial activity, the M1 was characterized by higher hydrophilicity and a smoother surface, thus reducing the overall surface area available to bacterial cell attachment and possibly leading to lower biofouling tendency and higher flux recovery ratio.

Stability and Release of Silver Ions. The robustness of the antibacterial and anti-biofouling activity of the functionalized membranes depends strongly on the controlled release

https://dx.doi.org/10.1021/acsami.0c13029
ACS Appl. Mater. Interfaces 2020, 12, 38285−38298

of silver.[19] The MOF nanorods act as reservoirs of silver, which slowly leak out into solution at the interface of the membrane and the feed solution or at the zone of biofilm attachment on the membrane surface. Therefore, the silver release rate was evaluated using ICP−mass spectrometry for 30 days for the nanocomposite membranes. Both membranes showed the same initial trend of increase in silver release rate in the first 7 days of monitoring (see Figure 11, illustrating the cumulative

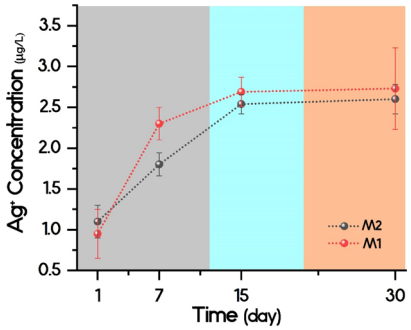

Figure 11. Silver-ion leaching from the nanocomposite membranes.

trend of Ag ions leakage), whereby the release rate in the 7 first days was more significant than in the following 8 days. The M1 sample showed a lower overall release rate compared to the M2 sample. This difference most probably stems from the much more concentrated presence of Ag-MOF close to the membrane surface for the M2 sample, as discussed above. Nevertheless, the overall release rate of silver ion for both membranes was low and finally reached approximate values of 2.6 and 2.7 μg/L for the M1 and M2 membranes, respectively.[10,22]

CONCLUSIONS

In this work, Ag-MOF nanorods were successfully synthesized and then embedded within the polyamide matrix of forward osmosis membranes to improve their antifouling and antibacterial properties. We fabricated novel Ag-MOF nanorods comprising amine functional groups, which interacted favorably with monomers during polyamide formation, as well as with polyamide chains themselves. This mechanism ensured the compatibility of Ag-MOF nanorods with the surrounding matrix and allowed suitable dispersion within the polyamide film without an adverse effect on the integrity of the selective layer. Two approaches were employed for fabricating nanocomposite membranes, one entailing the distribution of the nanorods in the aqueous solution during IP reaction, the other involving dispersion in the organic solution. In both cases, the results of membrane characterizations demonstrated the presence of Ag-MOF nanorods in the polyamide layer. The introduction of Ag-MOF nanorods increased the hydrophilicity of surface and resulted in the improved membranes' performance in forward osmosis. In addition, the nanocomposite membranes presented an excellent antifouling performance for both organic and biological foulants, presenting 84 and 73% flux recovery ratio following fouling and simple physical cleaning of the membrane. This effect was partly attributed to the observed antibacterial effect of Ag-MOF nanorods. The suitable incorporation of Ag-MOF nanorods within the polyamide matrix was also corroborated by slow leaching of silver in aqueous solution, suggesting the potential to impart prolonged activity during operation.

When comparing the two fabrication approaches, the results suggested that dispersing the nanorods in the organic TMC phase during fabrication produced a thicker and rougher membrane, with a large density of Ag-MOF embedded in the uppermost portion of the membrane selective layer. In contrast, dispersing the MOFs in the aqueous MPD solution likely slowed the diffusion of this monomer into the organic phase during IP, translating into a thinner and smoother selective layer incorporating nanorods in a more homogeneous fashion throughout the membrane cross-section. Ultimately, directly because of these phenomena, the M2 TFN membrane showed higher antibacterial activity, while the M1 presented overall better filtration performance and lower fouling-related flux declines owing to its properties comprising both suitable antibacterial properties and better hydrophilicity and surface smoothness.

ASSOCIATED CONTENT

Supporting Information

The Supporting Information is available free of charge at https://pubs.acs.org/doi/10.1021/acsami.0c13029.

Further detailed information on materials and methods, evaluation of the membrane transport properties, dynamic fouling experiments, fluorescent scanning microscopy, and quantification of the leakage of silver ions from the membrane, digital images of the MPD aqueous and TMC organic solutions immediately after the addition of Ag-MOF nanorods, FESEM images of the M1 membrane at different magnifications in secondary and backscatter modes, FESEM images of the M2 membrane at different magnifications in secondary and backscatter modes, high-magnification FESEM images of the M1 and M2 membranes in secondary and backscatter modes, and AFM images of the neat M0, M1, and M2 membranes (PDF)

AUTHOR INFORMATION

Corresponding Authors

Ahmad Rahimpour − *Department of Chemical Engineering, Babol Noshirvani University of Technology, Babol 4714781167, Iran;* orcid.org/0000-0003-1511-2761; Email: ahmadrahimpour@nit.ac.ir

Mark Elliott − *Department of Civil, Construction and Environmental Engineering, University of Alabama, Tuscaloosa, Alabama 35487, United States;* orcid.org/0000-0002-7835-0612; Email: melliott@eng.ua.edu

Authors

S. Fatemeh Seyedpour − *Department of Chemical Engineering, Babol Noshirvani University of Technology, Babol 4714781167, Iran*

Mostafa Dadashi Firouzjaei − *Department of Civil, Construction and Environmental Engineering, University of Alabama, Tuscaloosa, Alabama 35487, United States;* orcid.org/0000-0002-0215-8210

Ehsan Zolghadr − *Department of Physics and Astronomy, University of Alabama, Tuscaloosa, Alabama 35487, United States;* orcid.org/0000-0003-2876-8508

Ahmad Arabi Shamsabadi − *Department of Chemistry, University of Pennsylvania, Philadelphia, Pennsylvania 19104, United States;* orcid.org/0000-0002-9726-2466

https://dx.doi.org/10.1021/acsami.0c13029
ACS Appl. Mater. Interfaces 2020, 12, 38285−38298

Parnab Das − *Department of Civil, Construction and Environmental Engineering, University of Alabama, Tuscaloosa, Alabama 35487, United States*

Farhad Akbari Afkhami − *Department of Chemistry, The University of Alabama, Tuscaloosa, Alabama 35487, United States;* orcid.org/0000-0001-5977-8480

Mohtada Sadrzadeh − *Department of Mechanical Engineering, 10-367 Donadeo Innovation Center for Engineering, Advanced Water Research Lab (AWRL), University of Alberta, Edmonton, Alberta T6G 1H9, Canada;* orcid.org/0000-0002-0403-8351

Alberto Tiraferri − *Department of Environment, Land and Infrastructure Engineering (DIATI), Politecnico di Torino, Turin 10129, Italy;* orcid.org/0000-0001-9859-1328

Complete contact information is available at: https://pubs.acs.org/10.1021/acsami.0c13029

Author Contributions

[∇]S.F.S. and M.D.F. contributed equally to this work.

Notes

The authors declare no competing financial interest.

■ ACKNOWLEDGMENTS

M.D.F., P.D., and M.E. thank University of Alabama's support. A.R. and A.T. acknowledge Babol Noshirvani University of Technology and Politecnico di Torino and for their support. M.S. thanks the NSERC—Natural Sciences and Engineering Research Council of Canada (CRDPJ 501857-16) for financial support.

■ REFERENCES

(1) Saqib, J.; Aljundi, I. H. Membrane fouling and modification using surface treatment and layer-by-layer assembly of polyelectrolytes: state-of-the-art review. *J. Water Process Eng.* **2016**, *11*, 68−87.

(2) Esfahani, M. R.; Aktij, S. A.; Dabaghian, Z.; Firouzjaei, M. D.; Rahimpour, A.; Eke, J.; Escobar, I. C.; Abolhassani, M.; Greenlee, L. F.; Esfahani, A. R.; Sadmani, A.; Koutahzadeh, N. Nanocomposite membranes for water separation and purification: Fabrication, modification, and applications. *Sep. Purif. Technol.* **2019**, *213*, 465−499.

(3) Madaeni, S. S.; Hasankiadeh, N. T.; Kurdian, A. R.; Rahimpour, A. Modeling and optimization of membrane fabrication using artificial neural network and genetic algorithm. *Sep. Purif. Technol.* **2010**, *76*, 33−43.

(4) Kebria, M. R. S.; Rahimpour, A.; Salestan, S. K.; Seyedpour, S. F.; Jafari, A.; Banisheykholeslami, F.; Tavajohi Hassan Kiadeh, N. Hyper-branched dendritic structure modified PVDF electrospun membranes for air gap membrane distillation. *Desalination* **2020**, *479*, 114307.

(5) Firouzjaei, M. D.; Seyedpour, S. F.; Aktij, S. A.; Giagnorio, M.; Bazrafshan, N.; Mollahosseini, A.; Samadi, F.; Ahmadalipour, S.; Firouzjaei, F. D.; Esfahani, M. R. Recent advances in functionalized polymer membranes for biofouling control and mitigation in forward osmosis. *J. Membr. Sci.* **2020**, *596*, 117604.

(6) Mozafari, M.; Seyedpour, S. F.; Salestan, S. K.; Rahimpour, A.; Shamsabadi, A. A.; Firouzjaei, M. D.; Esfahani, M. R.; Tiraferri, A.; Mohsenian, H.; Sangermano, M.; Soroush, M. Facile Cu-BTC surface modification of thin chitosan film coated polyethersulfone membranes with improved antifouling properties for sustainable removal of manganese. *J. Membr. Sci.* **2019**, *588*, 117200.

(7) Mohammadi, G.; Jahanshahi, M.; Rahimpour, A. Fabrication and evaluation of Nafion nanocomposite membrane based on ZrO2−TiO2 binary nanoparticles as fuel cell MEA. *Int. J. Hydrogen Energy* **2013**, *38*, 9387−9394.

(8) Esfahani, M. R.; Koutahzadeh, N.; Esfahani, A. R.; Firouzjaei, M. D.; Anderson, B.; Peck, L. A novel gold nanocomposite membrane with enhanced permeation, rejection and self-cleaning ability. *J. Membr. Sci.* **2019**, *573*, 309−319.

(9) Hermans, S.; Mariën, H.; Van Goethem, C.; Vankelecom, I. F. Recent developments in thin film (nano)composite membranes for solvent resistant nanofiltration. *Curr. Opin. Chem. Eng.* **2015**, *8*, 45−54.

(10) Rahimpour, A.; Seyedpour, S. F.; Aghapour Aktij, S.; Dadashi Firouzjaei, M.; Zirehpour, A.; Arabi Shamsabadi, A.; Khoshhal Salestan, S.; Jabbari, M.; Soroush, M. Simultaneous Improvement of Antimicrobial, Antifouling, and Transport Properties of Forward Osmosis Membranes with Immobilized Highly-Compatible Polyrhodanine Nanoparticles. *Environ. Sci. Technol.* **2018**, *52*, 5246−5258.

(11) Zirehpour, A.; Rahimpour, A.; Khoshhal, S.; Firouzjaei, M. D.; Ghoreyshi, A. A. The impact of MOF feasibility to improve the desalination performance and antifouling properties of FO membranes. *RSC Adv.* **2016**, *6*, 70174−70185.

(12) Kim, I.-C.; Jeong, B.-R.; Kim, S.-J.; Lee, K.-H. Preparation of high flux thin film composite polyamide membrane: the effect of alkyl phosphate additives during interfacial polymerization. *Desalination* **2013**, *308*, 111−114.

(13) Pejman, M.; Firouzjaei, M. D.; Aktij, S. A.; Das, P.; Zolghadr, E.; Jafarian, H.; Shamsabadi, A. A.; Elliott, M.; Esfahani, M. R.; Sangermano, M.; Sadrzadeh, M.; Wujcik, E. K.; Rahimpour, A.; Tiraferri, A. Improved antifouling and antibacterial properties of forward osmosis membranes through surface modification with zwitterions and silver-based metal organic frameworks. *J. Membr. Sci.* **2020**, *611*, 118352.

(14) Mollahosseini, A.; Rahimpour, A. A new concept in polymeric thin-film composite nanofiltration membranes with antibacterial properties. *Biofouling* **2013**, *29*, 537−548.

(15) Tang, C.; Li, X.; Li, Z.; Hao, J. Interfacial Hydrogen Bonds and Their Influence Mechanism on Increasing the Thermal Stability of Nano-SiO2-Modified Meta-Aramid Fibres. *Polymers* **2017**, *9*, 504.

(16) Seyedpour, S. F.; Rahimpour, A.; Esfahani, M. R. Methods of making nanostructured metal-organic frameworks. U.S. Patent 20,200,079,796 A1, 2020.

(17) Firouzjaei, M. D.; Afkhami, F. A.; Esfahani, M. R.; Turner, C. H.; Nejati, S. Experimental and molecular dynamics study on dye removal from water by a graphene oxide-copper-metal organic framework nanocomposite. *J. Water Process Eng.* **2020**, *34*, 101180.

(18) Seyedpour, S. F.; Rahimpour, A.; Najafpour, G. Facile in-situ assembly of silver-based MOFs to surface functionalization of TFC membrane: A novel approach toward long-lasting biofouling mitigation. *J. Membr. Sci.* **2019**, *573*, 257−269.

(19) Wyszogrodzka, G.; Marszałek, B.; Gil, B.; Dorożyński, P. Metal-organic frameworks: mechanisms of antibacterial action and potential applications. *Drug Discovery Today* **2016**, *21*, 1009−1018.

(20) Pejman, M.; Dadashi Firouzjaei, M.; Aghapour Aktij, S.; Das, P.; Zolghadr, E.; Jafarian, H.; Arabi Shamsabadi, A.; Elliott, M. A.; Sadrzadeh, M.; Sangermano, M.; Rahimpour, A.; Tiraferri, A. In Situ Ag-MOF Growth on Pre-Grafted Zwitterions Imparts Outstanding Antifouling Properties to Forward Osmosis Membranes. *ACS Appl. Mater. Interfaces* **2020**, DOI: 10.1021/acsami.0c12141.

(21) Li, J.; Wang, H.; Yuan, X.; Zhang, J.; Chew, J. W. Metal-organic framework membranes for wastewater treatment and water regeneration. *Coord. Chem. Rev.* **2020**, *404*, 213116.

(22) Firouzjaei, M. D.; Shamsabadi, A. A.; Aktij, S. A.; Seyedpour, S. F.; Sharifian Gh, M.; Rahimpour, A.; Esfahani, M. R.; Ulbricht, M.; Soroush, M. Exploiting Synergetic Effects of Graphene Oxide and a Silver-Based Metal−Organic Framework To Enhance Antifouling and Anti-Biofouling Properties of Thin-Film Nanocomposite Membranes. *ACS Appl. Mater. Interfaces* **2018**, *10*, 42967−42978.

(23) Tiraferri, A.; Kang, Y.; Giannelis, E. P.; Elimelech, M. Superhydrophilic thin-film composite forward osmosis membranes for organic fouling control: fouling behavior and antifouling mechanisms. *Environ. Sci. Technol.* **2012**, *46*, 11135−11144.

(24) Seyedpour, S. F.; Rahimpour, A.; Shamsabadi, A. A.; Soroush, M. Improved performance and antifouling properties of thin-film composite polyamide membranes modified with nano-sized bactericidal graphene quantum dots for forward osmosis. *Chem. Eng. Res. Des.* **2018**, *139*, 321−334.
(25) Yi, M.; Lau, C. H.; Xiong, S.; Wei, W.; Liao, R.; Shen, L.; Lu, A.; Wang, Y. Zwitterion−Ag Complexes That Simultaneously Enhance Biofouling Resistance and Silver Binding Capability of Thin Film Composite Membranes. *ACS Appl. Mater. Interfaces* **2019**, *11*, 15698−15708.
(26) Yin, J.; Zhu, G.; Deng, B. Graphene oxide (GO) enhanced polyamide (PA) thin-film nanocomposite (TFN) membrane for water purification. *Desalination* **2016**, *379*, 93−101.
(27) Baig, M. I.; Ingole, P. G.; Choi, W. K.; Jeon, J.-d.; Jang, B.; Moon, J. H.; Lee, H. K. Synthesis and characterization of thin film nanocomposite membranes incorporated with surface functionalized Silicon nanoparticles for improved water vapor permeation performance. *Chem. Eng. J.* **2017**, *308*, 27−39.
(28) Wei, X.; Wang, Z.; Wang, J.; Wang, S. A novel method of surface modification to polysulfone ultrafiltration membrane by preadsorption of citric acid or sodium bisulfite. *Membr. Water Treat.* **2012**, *3*, 35−49.
(29) Wu, Z.; Li, S.; Liu, M.; Wang, Z.; Liu, X. Liquid oxygen compatible epoxy resin: modification and characterization. *RSC Adv.* **2015**, *5*, 11325−11333.
(30) Firouzjaei, M. D.; Shamsabadi, A. A.; Sharifian Gh, M.; Rahimpour, A.; Soroush, M. A Novel Nanocomposite with Superior Antibacterial Activity: A Silver-Based Metal Organic Framework Embellished with Graphene Oxide. *Adv. Mater. Interfaces* **2018**, *5*, 1701365.
(31) Waterhouse, G. I. N.; Bowmaker, G. A.; Metson, J. B. The thermal decomposition of silver (I, III) oxide: A combined XRD, FT-IR and Raman spectroscopic study. *Phys. Chem. Chem. Phys.* **2001**, *3*, 3838−3845.
(32) Perera, D. H. N.; Song, Q.; Qiblawey, H.; Sivaniah, E. Regulating the aqueous phase monomer balance for flux improvement in polyamide thin film composite membranes. *J. Membr. Sci.* **2015**, *487*, 74−82.
(33) Ali, M. E. A.; Wang, L.; Wang, X.; Feng, X. Thin film composite membranes embedded with graphene oxide for water desalination. *Desalination* **2016**, *386*, 67−76.
(34) Bano, S.; Mahmood, A.; Kim, S.-J.; Lee, K.-H. Graphene oxide modified polyamide nanofiltration membrane with improved flux and antifouling properties. *J. Mater. Chem. A* **2015**, *3*, 2065−2071.
(35) Saha, N. K.; Joshi, S. V. Performance evaluation of thin film composite polyamide nanofiltration membrane with variation in monomer type. *J. Membr. Sci.* **2009**, *342*, 60−69.
(36) Khorshidi, B.; Thundat, T.; Fleck, B. A.; Sadrzadeh, M. Thin film composite polyamide membranes: parametric study on the influence of synthesis conditions. *RSC Adv.* **2015**, *5*, 54985−54997.
(37) Wei, X.; Wang, Z.; Wang, J.; Wang, S. A novel method of surface modification to polysulfone ultrafiltration membrane by preadsorption of citric acid or sodium bisulfite. *Membr. Water Treat.* **2012**, *3*, 35−49.
(38) Liu, R.; Xian, Z.; Zhang, S.; Chen, C.; Yang, Z.; Li, H.; Zheng, W.; Zhang, G.; Cao, H. Electrochemical-reduction-assisted assembly of ternary Ag nanoparticles/polyoxometalate/graphene nanohybrids and their activity in the electrocatalysis of oxygen reduction. *RSC Adv.* **2015**, *5*, 74447−74456.
(39) Park, S.-H.; Kim, S. H.; Park, S.-J.; Ryoo, S.; Woo, K.; Lee, J. S.; Kim, T.-S.; Park, H.-D.; Park, H.; Park, Y.-I.; Cho, J.; Lee, J.-H. Direct incorporation of silver nanoparticles onto thin-film composite membranes via arc plasma deposition for enhanced antibacterial and permeation performance. *J. Membr. Sci.* **2016**, *513*, 226−235.
(40) Khorshidi, B.; Thundat, T.; Fleck, B. A.; Sadrzadeh, M. A novel approach toward fabrication of high performance thin film composite polyamide membranes. *Sci. Rep.* **2016**, *6*, 22069.
(41) Liu, Z.; Ou, J.; Wang, H.; You, X.; Ye, M. Synthesis and characterization of hydrazide-linked and amide-linked organic polymers. *ACS Appl. Mater. Interfaces* **2016**, *8*, 32060−32067.
(42) Wagner, C.; Naumkin, A.; Kraut-Vass, A.; Allison, J.; Powell, C.; Rumble, J., Jr. *NIST X-ray Photoelectron Spectroscopy Database, NIST Standard Reference Database 20*, version 3.4 (Web Version); U.S. Department of Commerce, 2003.
(43) Sun, Y.; Hu, J.; An, S.; Zhang, Q.; Guo, Y.; Song, D.; Shang, Q. Selective esterification of glycerol with acetic acid or lauric acid over rod-like carbon-based sulfonic acid functionalized ionic liquids. *Fuel* **2017**, *207*, 136−145.
(44) Kim, S.; Yun, Y.-S.; Choi, Y.-E. Development of waste biomass based sorbent for removal of cyanotoxin microcystin-LR from aqueous phases. *Bioresour. Technol.* **2018**, *247*, 690−696.
(45) Beamson, G. *High Resolution XPS of Organic Polymers. The Scienta ESCA 300 Database*; Wiley, 1992.
(46) Benavente, J.; Vázquez, M. I. Effect of age and chemical treatments on characteristic parameters for active and porous sublayers of polymeric composite membranes. *J. Colloid Interface Sci.* **2004**, *273*, 547−555.
(47) Ariza, M. J.; Benavente, J.; Rodríguez-Castellón, E.; Palacio, L. Effect of hydration of polyamide membranes on the surface electrokinetic parameters: surface characterization by X-ray photoelectronic spectroscopy and atomic force microscopy. *J. Colloid Interface Sci.* **2002**, *247*, 149−158.
(48) Khorshidi, B.; Biswas, I.; Ghosh, T.; Thundat, T.; Sadrzadeh, M. Robust fabrication of thin film polyamide-TiO 2 nanocomposite membranes with enhanced thermal stability and anti-biofouling propensity. *Sci. Rep.* **2018**, *8*, 784.
(49) Tiraferri, A.; Kang, Y.; Giannelis, E. P.; Elimelech, M. Highly hydrophilic thin-film composite forward osmosis membranes functionalized with surface-tailored nanoparticles. *ACS Appl. Mater. Interfaces* **2012**, *4*, 5044−5053.
(50) Echlin, P.; Fiori, C.; Goldstein, J.; Joy, D. C.; Newbury, D. E. *Advanced Scanning Electron Microscopy and X-ray Microanalysis*; Springer Science & Business Media, 2013.
(51) Sadeghi, M.; Arabi Shamsabadi, A.; Ronasi, A.; Isfahani, A. P.; Dinari, M.; Soroush, M. Engineering the dispersion of nanoparticles in polyurethane membranes to control membrane physical and transport properties. *Chem. Eng. Sci.* **2018**, *192*, 688−698.
(52) Zhao, Q.; Hou, J.; Shen, J.; Liu, J.; Zhang, Y. Long-lasting antibacterial behavior of a novel mixed matrix water purification membrane. *J. Mater. Chem. A* **2015**, *3*, 18696−18705.
(53) Song, X.; Zhou, Q.; Zhang, T.; Xu, H.; Wang, Z. Pressure-assisted preparation of graphene oxide quantum dot-incorporated reverse osmosis membranes: antifouling and chlorine resistance potentials. *J. Mater. Chem. A* **2016**, *4*, 16896−16905.
(54) Xia, S.; Yao, L.; Zhao, Y.; Li, N.; Zheng, Y. Preparation of graphene oxide modified polyamide thin film composite membranes with improved hydrophilicity for natural organic matter removal. *Chem. Eng. J.* **2015**, *280*, 720−727.
(55) Tang, C. Y.; Kwon, Y.-N.; Leckie, J. O. Effect of membrane chemistry and coating layer on physiochemical properties of thin film composite polyamide RO and NF membranes: II. Membrane physiochemical properties and their dependence on polyamide and coating layers. *Desalination* **2009**, *242*, 168−182.
(56) Kang, G.-d.; Cao, Y.-m. Development of antifouling reverse osmosis membranes for water treatment: a review. *Water Res.* **2012**, *46*, 584−600.
(57) Asadollahi, M.; Bastani, D.; Musavi, S. A. Enhancement of surface properties and performance of reverse osmosis membranes after surface modification: a review. *Desalination* **2017**, *420*, 330−383.
(58) Al-Amoudi, A.; Lovitt, R. W. Fouling strategies and the cleaning system of NF membranes and factors affecting cleaning efficiency. *J. Membr. Sci.* **2007**, *303*, 4−28.
(59) Schwegmann, H.; Feitz, A. J.; Frimmel, F. H. Influence of the zeta potential on the sorption and toxicity of iron oxide nanoparticles on S. cerevisiae and E. coli. *J. Colloid Interface Sci.* **2010**, *347*, 43−48.

https://dx.doi.org/10.1021/acsami.0c13029
ACS Appl. Mater. Interfaces 2020, 12, 38285−38298

(60) Childress, A. E.; Elimelech, M. Effect of solution chemistry on the surface charge of polymeric reverse osmosis and nanofiltration membranes. *J. Membr. Sci.* **1996**, *119*, 253−268.
(61) Zhao, M.; Fu, S.; Zhang, H.; Huang, H.; Wei, Y.; Zhang, Y. Enhanced separation and antifouling performance of reverse osmosis membrane incorporated with carbon nanotubes functionalized by atom transfer radical polymerization. *RSC Adv.* **2017**, *7*, 46969−46979.
(62) Tiraferri, A.; Yip, N. Y.; Straub, A. P.; Romero-Vargas Castrillon, S.; Elimelech, M. A method for the simultaneous determination of transport and structural parameters of forward osmosis membranes. *J. Membr. Sci.* **2013**, *444*, 523−538.
(63) Phillip, W. A.; Yong, J. S.; Elimelech, M. Reverse draw solute permeation in forward osmosis: modeling and experiments. *Environ. Sci. Technol.* **2010**, *44*, 5170−5176.
(64) Zirehpour, A.; Rahimpour, A.; Seyedpour, F.; Jahanshahi, M. Developing new CTA/CA-based membrane containing hydrophilic nanoparticles to enhance the forward osmosis desalination. *Desalination* **2015**, *371*, 46−57.
(65) Lind, M. L.; Ghosh, A. K.; Jawor, A.; Huang, X.; Hou, W.; Yang, Y.; Hoek, E. M. V. Influence of zeolite crystal size on zeolite-polyamide thin film nanocomposite membranes. *Langmuir* **2009**, *25*, 10139−10145.
(66) Huang, H.; Ying, Y.; Peng, X. Graphene oxide nanosheet: an emerging star material for novel separation membranes. *J. Mater. Chem. A* **2014**, *2*, 13772−13782.
(67) Lee, S. Y.; Kim, H. J.; Patel, R.; Im, S. J.; Kim, J. H.; Min, B. R. Silver nanoparticles immobilized on thin film composite polyamide membrane: characterization, nanofiltration, antifouling properties. *Polym. Adv. Technol.* **2007**, *18*, 562−568.
(68) Yin, J.; Yang, Y.; Hu, Z.; Deng, B. Attachment of silver nanoparticles (AgNPs) onto thin-film composite (TFC) membranes through covalent bonding to reduce membrane biofouling. *J. Membr. Sci.* **2013**, *441*, 73−82.
(69) Seyedpour, S. F.; Arabi Shamsabadi, A.; Khoshhal Salestan, S.; Dadashi Firouzjaei, M.; Sharifian Gh, M.; Rahimpour, A.; Akbari Afkhami, F.; Shirzad Kebria, M. R.; Elliott, M. A.; Tiraferri, A.; Sangermano, M.; Esfahani, M. R.; Soroush, M. Tailoring the Biocidal Activity of Novel Silver-Based Metal Azolate Frameworks. *ACS Sustainable Chem. Eng.* **2020**, *8*, 7588−7599.
(70) Lu, X.; Ye, J.; Zhang, D.; Xie, R.; Bogale, R. F.; Sun, Y.; Zhao, L.; Zhao, Q.; Ning, G. Silver carboxylate metal−organic frameworks with highly antibacterial activity and biocompatibility. *J. Inorg. Biochem.* **2014**, *138*, 114−121.
(71) Berchel, M.; Le Gall, T.; Denis, C.; Le Hir, S.; Quentel, F.; Elléouet, C.; Montier, T.; Rueff, J.-M.; Salaün, J.-Y.; Haelters, J.-P.; Hix, G. B.; Lehn, P.; Jaffrès, P.-A. A silver-based metal−organic framework material as a "reservoir" of bactericidal metal ions. *New J. Chem.* **2011**, *35*, 1000−1003.
(72) Rueff, J.-M.; Perez, O.; Caignaert, V.; Hix, G.; Berchel, M.; Quentel, F.; Jaffrès, P.-A. Silver-Based Hybrid Materials from meta- or para-Phosphonobenzoic Acid: Influence of the Topology on Silver Release in Water. *Inorg. Chem.* **2015**, *54*, 2152−2159.
(73) Zhu, J.; Hou, J.; Zhang, Y.; Tian, M.; He, T.; Liu, J.; Chen, V. Polymeric antimicrobial membranes enabled by nanomaterials for water treatment. *J. Membr. Sci.* **2018**, *550*, 173−197.
(74) Chamakura, K.; Perez-Ballestero, R.; Luo, Z.; Bashir, S.; Liu, J. Comparison of bactericidal activities of silver nanoparticles with common chemical disinfectants. *Colloids Surf., B* **2011**, *84*, 88−96.
(75) Shen, L.; Zhang, X.; Zuo, J.; Wang, Y. Performance enhancement of TFC FO membranes with polyethyleneimine modification and post-treatment. *J. Membr. Sci.* **2017**, *534*, 46−58.

https://dx.doi.org/10.1021/acsami.0c13029
ACS Appl. Mater. Interfaces 2020, 12, 38285−38298